HHS Public Access

Author manuscript

Nat Genet. Author manuscript; available in PMC 2010 August 01.

Published in final edited form as:

Nat Genet. 2010 February ; 42(2): 175–180. doi:10.1038/ng.519.

AHI1 is required for outer segment development and is a modifier for retinal degeneration in nephronophthisis

Carrie M Louie[1], **Gianluca Caridi**[2], **Vanda S Lopes**[3,4], **Francesco Brancati**[5], **Andreas Kispert**[6], **Madeline A Lancaster**[1], **Andrew M Schlossman**[1], **Edgar A Otto**[7], **Michael Leitges**[8], **Hermann-Josef Groene**[9], **Irma Lopez**[10], **Harini V Gudiseva**[11], **John F O'Toole**[7], **Elena Vallespin**[12], **Radha Ayyagari**[11], **Carmen Ayuso**[12], **Frans P Cremers**[13], **Anneke I den Hollander**[13], **Robert K Koenekoop**[10], **Bruno Dallapiccola**[5], **Gian Marco Ghiggeri**[2], **Friedhelm Hildebrandt**[7], **Enza Maria Valente**[5,14], **David S Williams**[3,4], and **Joseph G Gleeson**[1,*]

[1]Neurogenetics Laboratory, Howard Hughes Medical Institute, Department of Pediatrics, University of California, San Diego, La Jolla, California, USA, 92093. [2]Laboratorio di Fisiopatologia dell'Uremia, Istituto Giannina Gaslini IRCCS, 16148 Genova, Italy [3]Departments of Ophthalmology and Neurobiology, Jules Stein Eye Institute, University of California, Los Angeles School of Medicine, Los Angeles, CA 90095. [4]Department of Pharmacology, University of California, San Diego, La Jolla, CA, USA, 92093. [5]CSS-Mendel Institute, Casa Sollievo della Sofferenza Hospital, viale Regina Margherita 261, 00198 Rome, Italy. [6]Institut für Molekularbiologie, Medizinische Hochschule Hannover, 30625 Hannover, Germany [7]Departments of Pediatrics and of Human Genetics, Howard Hughes Medical Institute, University of Michigan, Ann Arbor, MI 48109, USA. [8]The Biotechnology Centre of Oslo, University of Oslo, Oslo, Norway [9]Department of Cellular and Molecular Pathology, German Cancer Research Center, 69120 Heidelberg, Germany. [10]McGill Ocular Genetics Laboratory, McGill University Health Centre, Montreal, Quebec, H3H 1P3, Canada. [11]Department of Ophthalmology, University of California at San Diego, La Jolla, CA, USA 92093. [12]Department of Medical Genetics, Fundación Jiménez-Díaz, Madrid, 28040, CIBERER, Spain [13]Department of Human Genetics, University Nijmegen Medical Centre, Nijmegen Centre for Molecular Life Sciences, Radboud, 6500 HB Nijmegen, The Netherlands [14]Dept. of Medical and Surgical Pediatric Sciences, University of Messina, 98100 Messina, Italy

Abstract

Photoreceptor degeneration is a common feature of ciliopathies, owing to the importance of the highly specialized ciliary structure of these cells. Absence of *AHI1*, which encodes a cilium-

*To whom correspondence should be addressed at: jogleeson@ucsd.edu.

Author Contributions C.M.L and J.G.G. designed the study and experiments with significant contributions from D.S.W. C.M.L, A.K., F.H. and M.L. developed mutant mice and C.M.L., E.A.O., F.H., H.G. performed initial characterization. C.M.L. performed murine experiments. V.S.L. performed electron microscopy. G.C., E.M.V., and G.M.G. ascertained and supervised genotyping of human cases and contributed to analysis. A.I.dH., R.K.K., F.P.C. contributed LCA samples and screened a portion of LCA cases. C.A., R.A., G.V., E.V. contributed samples for the LCA study. F.B, I.L., A.S., and C.M.L. performed genetic screening and genotyping. M.A.L. performed biochemical assays. C.M.L. and J.G.G. wrote the manuscript with contributions from E.M.V., G.C, D.S.W., V.S.L., F.H., F.B., and A.K.

localized protein, has been shown to cause a form of Joubert syndrome highly penetrant for retinal degeneration[1,2]. We show that *Ahi1* knockout mice fail to form outer segments (OS), and show abnormal distribution of opsin throughout photoreceptors. Apoptotic cell death occurs rapidly between 2-4 weeks of age and is significantly delayed by reduced dosage of opsin. This phenotype also displays dosage-sensitive genetic interactions with *Nphp1*, another ciliopathy gene. Although not a primary cause of retinal blindness in humans, an allele of *AHI1* modifies the relative risk of retinal degeneration greater than 7 fold within a nephronophthisis cohort. Our data support context-specific roles for *AHI1* as a contributor to retinopathy and may explain a proportion of the variability of retinal phenotypes observed in nephronophthisis.

Ciliopathies comprise an increasingly diverse group of genetic disorders, united by their connection to primary cilia and/or basal body dysfunction[3]. Because of the pervasiveness of this organelle, these disorders manifest in numerous organs. Joubert syndrome (JS, *i.e.* cerebellar hypoplasia), Leber congenital amaurosis (LCA, *i.e.* congenital retinal blindness) and nephronophthisis (NPHP, *i.e.* fibrocystic renal disease) primarily affect three organs frequently diseased in ciliopathies, namely cerebellum, retina and kidney. These diseases are highly genetically heterogeneous and are sometimes variable even within single families, undermining the predictive value of diagnostics and genetic counseling. Though many causative genes have been identified for these Mendelian disorders, our current understanding of the genetics and potential mechanisms is insufficient to explain this variability, and suggests involvement of genetic modifiers.

Mutations in *AHI1* are identified in 12% of patients with JS and 20% of patients with JS + LCA[1,2,4,5], though *AHI1* mutations are not known to cause non-syndromic LCA. AHI1 protein, or jouberin, contains an N-terminal coiled-coil region, seven WD40 repeats and an SH3 domain[6] and interacts with nephrocystin-1 (NPHP1)[7], the gene for which is the most commonly mutated in juvenile NPHP[8,9]. To study *AHI1* in ciliopathogenesis, we generated targeted conditional and null alleles of murine *Ahi1*, flanking exons 6-7 with loxP sequences (Supplementary Fig. 1a). Homozygous germline mutants were runted and exhibited high mortality (Supplementary Fig. 1c,d). Brain morphology was grossly preserved and neuronal-specific conditional knockouts (*Ahi1 Nestin cKO*) showed nearly Mendelian ratios at weaning age (data not shown), suggesting effects outside of the nervous system on survival.

Histological analysis of the retina revealed rapid loss of the outer nuclear (photoreceptor) layer with few nuclei remaining by age one month in *Ahi1* germline null mice ($Ahi1^{-/-}$, Fig. 1a). As early as P10, transmission electron microscopy showed complete absence of both rod and cone outer segments (OS, specialized disk-shaped membranes of photoreceptor cilia, Fig. 1b, and Supplementary Fig. 2a). This well-preceded the initiation of apoptotic cell death, apparent by ~3 weeks of age, as indicated by activated caspase-3 expression (Fig. 1c). Photoreceptor ciliary axonemes were intact and had normal 9+0 microtubule doublet configuration (Fig. 1b, Supplementary Fig. 2b), arguing against a role in axonemal development. Dark-adapted electroretinograms (ERG) from Nestin-Cre conditional mutants (*Ahi1 Nestin cKO*) and controls preceding cell loss confirmed absence of activity (Fig. 1d). Consistent with its putative role in cilia function, we found Ahi1 was enriched at the connecting cilium and basal body, and overlapped with centrin-2 (centriole/transition zone

marker[10],[11]) transgene expression (Fig. 1e). This expression pattern was reminiscent of ciliary transport molecules such as Ift88[12] and also other ciliopathy-associated molecules like Nphp1[13]. These results reveal specific defects of OS morphogenesis and photoreceptor survival associated with absence of *Ahi1*.

Rhodopsin (rod opsin and cofactor, retinal), responsible for initiating the first steps in light-dependant signal transduction, is also necessary for OS formation[14]-[17]. Disruptions of genes required for ciliary transport result in mislocalized opsin and OS defects[12],[18]-[20], prompting us to test for opsin localization in *Ahi1*$^{-/-}$ retina. We found severely disturbed opsin distribution as early as P10 (Fig. 2a). We quantified this in immunogold-labeled sections, which showed significantly increased inner segment labeling in mutants, both in the cytoplasm (IS) and particularly, along inner segment plasma membranes vs. controls (PM, Fig. 2b **and** Supplementary Fig. 2c). This difference was ~10-fold for both IS and PM (*P*= 8.0E-06 and 2.2E-07, respectively). Some other proteins implicated in OS morphogenesis appeared grossly intact (Supplementary Fig. 2d). We conclude opsin is significantly mis-accumulated in *Ahi1*$^{-/-}$ mice at an early stage of OS morphogenesis.

To further test for cell-type-specific requirements for *Ahi1* in opsin distribution, we used *Ahi1*$^{flox/flox}$ mice in a series of retinal *in vivo* electroporation experiments performed at P0 (Supplementary Fig. 3a). The pCAG-Cre:GFP vector drives Cre:GFP under the constitutive chick beta-actin promoter, and was used with pDsRed-CALNL recombination reporter[21],[22]. Photoreceptors with evidence of Cre recombination based upon expression of DsRed also showed recapitulation of the opsin redistribution phenotype by one month of age (Supplementary Fig. 3b), indicating a requirement for *Ahi1* in photoreceptors. To test for temporal-specific requirements for *Ahi1*, these experiments were repeated using instead pCAG-ERT2CreERT2, which activates Cre under control of 4-hydroxytamoxifen (4-OHT)[22]. Following 4-OHT dosage at P14, after the peak of OS development, we did not detect opsin accumulation at 2 and 4 weeks past Cre induction, despite evidence of recombination based upon expression of DsRed (*n*=2, Supplementary Fig. 3c,d). We conclude Ahi1 displays temporal specificity in its function in photoreceptors, possibly akin to the time dependance reported for ciliary transport machinery in kidney phenotypes[23]. These data also suggest other factors might be contributing to OS developmental defects in this model.

Mislocalized opsin is frequently associated with retinal degeneration in animal models[19],[24], and has been indicated as a major cause of photoreceptor cell death in the absence of heterotrimeric kinesin-2 function (D. Jimeno, V.S. Lopes, K. Khanobdee, X. Song, B. Chen, S. Nusinowitz, D.S. Williams, unpublished data). Because of the striking accumulation of opsin in *Ahi1*$^{-/-}$ mice, we hypothesized this might similarly contribute to cell death in *Ahi1*$^{-/-}$ photoreceptors. To test this directly, we reduced opsin levels in *Ahi1*$^{-/-}$ mice by introducing a rod opsin null allele[15] into the *Ahi1*$^{-/-}$ background. *Rho*$^{+/-}$ photoreceptors have approximately 40-50% reduction in opsin content[15],[25]. Reduction in opsin dosage did not affect OS formation, showing similar absence of OS in *Ahi1*$^{-/-}$*Rho*$^{+/-}$ compared to *Ahi1*$^{-/-}$ (Supplementary Fig. 4), but significantly delayed the cell loss seen in the *Ahi1*$^{-/-}$. We found nearly complete rescue of cell numbers at three weeks of age (*n*=3-7, *P*=0.00175) and partial rescue at one month (Fig. 3, *n*=3-4, *P*=0.00613). These data support the

hypothesis that abnormal accumulation of opsin contributes to the loss of *Ahi1*$^{-/-}$ photoreceptors.

Mutations in *NPHP1* cause juvenile nephronophthisis with partially penetrant retinopathy. To study *Nphp1* in the mouse, we generated a targeted disruption of *Nphp1* by insertion of a neobpA cassette into exon 4, generating a null allele, and confirmed absence of Nphp1 expression (Supplementary Fig. 5a,b,c). The photoreceptors of *Nphp1*$^{neo/neo}$ mice (hereafter denoted as *Nphp1*$^{-/-}$) formed OSs but underwent gradual retinal degeneration, slightly evident at 2 months (Supplementary Fig. 5d). This was milder than an independently targeted *Nphp1* mutant reported to show failure of OS formation followed by retinal degeneration[26]. Since both *Nphp1* alleles are predicted to function as nulls, this difference in severity of retinal phenotypes suggests the influence of genetic modifiers.

To test whether genetic interaction of *Ahi1* and *Nphp1* can influence phenotypic expression *in vivo*, we examined double mutant combinations of *Ahi1* and *Nphp1*, ranging from single heterozygotes to knockout; heterozygote combinations, for outer nuclear layer (ONL) thickness and for mislocalized opsin. To efficiently obtain genotypes homozygous null for *Ahi1*, we used the *Ahi1*^{flox} allele and the distal (peripheral) retina-specific Pax6α-Cre transgene[27] to circumvent the lethality issues associated with *Ahi1*$^{-/-}$. We observed trends of increasing severity of cell loss and opsin redistribution with additional deleterious alleles, with the *Ahi1* null allele showing a stronger effect (Fig. 4a). Specifically we found significantly decreased ONL thickness and increased ONL-localized opsin when we compared *Nphp1*$^{-/-}$*Ahi1*$^{+/-}$ against *Nphp1*$^{-/-}$ and *Ahi1*$^{+/-}$ controls at P21 (Fig. 4b). The data suggest dosage sensitive genetic interactions between *Ahi1* and *Nphp1* in retinal development.

Based on the pronounced retinopathy in *Ahi1*$^{-/-}$ mice, we next tested whether *AHI1* was mutated in humans with isolated LCA. In a screen of *AHI1* coding exons from well-characterized LCA patients (US, Canada, Netherlands, Spain, prescreened for known genes; *n*=176), no homozygous or compound heterozygous deleterious changes were identified, but one variant, p.R830W/c.C2488T, heterozygous in 9 independent cases, was of particular interest, though not significantly enriched (data not shown). In addition to conservation of p.R830 throughout vertebrate homologs, a change from arginine to tryptophan (from a polar basic residue to a nonpolar hydrophobic residue) is predicted to be damaging (Polyphen[28], SNPs3D[29]). This coupled with its position within the WD40 repeat domain (between two blades of its predicted propeller structure, Supplementary Fig. 6a,b) suggests this mutation may interfere with the function of AHI1, perhaps in protein-protein interactions.

To test whether this change altered sedimentation of AHI1 complexes *in vitro*, we expressed GFP-AHI1^{R830W}, GFP-AHI1^{WT} or GFP-EV (empty vector) in HEK293T cells with untagged human rhodopsin[30] (RHO) and assayed lysates by sucrose density gradients (Supplementary Fig. 6c). We identified two distinct sedimentation peaks containing AHI1 which appeared at lower intensity for GFP-AHI1^{R830W} transfected cells, suggesting underrepresentation of p.R830W in complexes, despite comparable total expression levels of p.R830W in HEK293T cells (Supplementary Fig. 6d). Furthermore, opsin was shifted towards lower density complexes in cells expressing p.R830W vs. those expressing wildtype

AHI1 or empty vector. This supports potentially hypomorphic effects of p.R830W, perhaps in complex stability or formation. This variant has been mentioned as a polymorphism in several *AHI1* studies[1,2,31,32], but the effect of this change on retinal disease has not been explored. Due to the genetic interaction of *Ahi1* and *Nphp1* in mouse, and the variable association of retinal degeneration (RD) with nephronophthisis (Senior-Løken syndrome, SLSN[33]), we hypothesized that *AHI1* p.R830W might contribute to the risk of retinopathy in nephronophthisis patients.

We thus genotyped 153 independent nephronophthisis cases from Italy (of which 16 have RD), and 306 ethnically-matched healthy controls for the p.R830W (c.C2488T) change. We found the T allele frequency was significantly higher in patients with NPHP+RD versus NPHP patients excluded for RD (25% vs. 1.8%, P=5.36E-06, Table 1) and versus controls (25% vs. 2.8%, P=9.03E-06, Table 1). This translated to a relative risk of 7.5 (95% CI 4.0-11.2) associated with *AHI1* p.R830W for retinal degeneration within NPHP patients. To determine if this association depended upon the primary gene mutation, we repeated this analysis after subdividing cases into those with *NPHP1* mutations (either homozygous deletion or compound heterozygous mutation) vs. those without *NPHP1* mutations. p.R830W continued to be significantly associated with NPHP+RD irrespective of the primary mutation (Table 1).

To test for population stratification, we also examined transmission of p.R830W in this cohort[34] by genotyping parents of 117 available trios. We found 17 informative trios where one parent was heterozygous for c.C2488T. Although this sample size was too limited for full TDT analysis, we found the T allele was over-transmitted to NPHP+RD patients. Specifically, T was transmitted 100% of the time to NPHP+RD patients (n=7, P<0.01, chi-squared), but only 50% of the time to NPHP patients without RD (n=10, no significant difference from the null hypothesis). This association was apparent when evaluating single families; for example, in one family with three NPHP affecteds[33], p.R830W segregated only with the sibling displaying absent ERG response, while the others retained visual function. Our results support the role of *AHI1* as a modifier of retinal degeneration in the context of mutations leading to NPHP.

That this *AHI1* allele is associated with retinal disease in as much as half of SLSN patients in this Italian population, suggests other rarer mutations of *AHI1* may behave similarly. Results from the mouse model support a role for *Ahi1* in cilia-associated trafficking mechanisms, consistent with those of a recent study describing *Ahi1* in cultured cells[35]. We also identify a new role for *Ahi1* in photoreceptor development and demonstrate the utility of mouse genetic interaction in identifying loci conferring high risk alleles for disease. A similar effect was presented with one variant of RPGRIP1L[36], supporting the role of modifiers in phenotypic expressivity of ciliopathies. Given the complexity of ciliopathy phenotypes, it is likely other variable phenotypes could also be explained by modifiers. Intriguingly, a population of JS patients (n=155) did not reveal a significant difference in frequency of p.R830W although it was slightly higher relative to controls. These patients were ascertained for phenotypes associated with a specific constellation of midbrain-hindbrain malformations, but also variably present with renal and/or retinal dysfunction. Lack of significant association within JS may reflect more complex interactions at the

molecular level, requiring specific disruptions to alter phenotypic expression. Future screenings at other loci may help elucidate these distinct but overlapping mechanisms. Our example within the ciliopathies shows that mutational analysis of other causative genes from the broader clinical spectrum can yield substantial insight into the genetics and pathogenesis of heterogeneous syndromic disorders.

Online Methods

Subjects and mutational screening

Subjects were ascertained from populations of European ancestry (Italian, French/French Canadian, Spanish, Dutch) based on clinical features specific to LCA, NPH, and JSRD (exception of NPH group, mostly Italian). In particular, NPHP patients were ascertained over 15 years at the Nephrology Center of the G. Gaslini Childrens Hospital (Genoa, Italy)[37]. Diagnosis of NPHP was based on bio-clinical tests, kidney and liver ultrasound, ophthalmologic examination, and molecular tests (for *NPHP1* deletion and/or mutations). All patients showed clinical and laboratory signs of NPHP, including urinary concentration defect, increase of serum creatinine levels above the normal range for age, and small hyperechoic kidneys without cortico-medullary differentiation. >70% patients had already developed ESRF (End-Stage Renal Failure) and most with ESRF had been transplanted. Patients with possible neurological involvement underwent detailed neurological testing, including brain MRI and EEG. JSRD patients were ascertained through the International JSRD Study Group, referring patients from several countries worldwide. The clinical diagnosis was confirmed by brain neuroimaging showing the typical “molar tooth sign”. A standardized clinical questionnaire was obtained to assess extent of multiorgan involvement. Control subjects were drawn from the same populations and represent healthy subjects with respect to the clinical signs of interest. Informed consent was obtained for all subjects according to approved institutional human subjects protocols (Human Research Protection Program Committees of UCSD, La Jolla and CSS-Mendel Institute, Rome).

Exons were PCR-amplified and sequenced using BigDye Terminator chemistry (ABI Prism 3100), and chromatograms were analyzed visually; or PCR fragments were analyzed on a DHPLC-based WAVE DNA Fragment Analysis System (Transgenomic, Crewe, United Kingdom). Samples with abnormal elution profiles underwent direct bidirectional sequencing as above. Primer sequences were published previously[1].

Knockout and transgenic mice

Animals were used in compliance with approved Institutional Animal Care and Use Committee protocols.

Generation of Ahi1 mutant mice—*Ahi1* conditional (“flox”) and null allele mice were generated by targeted homologous recombination. The floxed region (containing exons 6-7), and flanking homology arms of *Ahi1* were PCR-amplified from 129/SvJ genomic DNA; flanked with SalI, BamHI, and XhoI restriction sites; and subcloned into the modified pflox vector[38](J. Marth) containing PGKneobpA (positive selection) and HSV-TK (negative selection). This was linearized with SbfI and transfected into 129SvJ-derived ES cells. G418

and gancyclovir resistant clones were selected, 9 correctly recombined ES clones were identified by Southern blot with two distinct probes, and two clones were injected into C57Bl/6 blastocysts. High percentage chimeras were bred to C57Bl/6 for germline transmission and to EIIa-Cre to generate mosaic Cre recombinants. Mosaics were bred to C57Bl/6 to isolate null and conditional alleles. Mice were genotyped by PCR in a multiplex reaction, amplifying a 206bp (null allele), a 297bp (wildtype) and/or a 399bp (conditional) product (Supplementary Table 1).

Generation of *Nphp1* mutant mice—To clone the mouse *Nphp1* locus, a 129/Ola genomic cosmid library (obtained from the Resourcenzentrum Berlin) was probed using the mouse cDNA. A single cosmid clone was purified, and a 10 kb *Sac*I and 12 kb EcoRI fragment harboring the exon 4 region of the *Nphp1* transcription unit were subcloned and characterized by restriction mapping. To generate targeting construct for *Nphp1*, a 12.5 kb genomic fragment derived from the two subfragments was modified by inserting a floxed PGK-neobpA cassette (*pMC1-neo-polyA*) into an unique NheI site. The targeting vector was linearized at a unique SalI site and introduced into E14 ES cells[39]. 159 G418-resistant colonies were screened by Southern blot analysis and four correctly targeted ES cell lines were identified. $Nphp1^{neo}$/+ ES cells (129/Ola) were microinjected into NMRI albino mouse blastocysts to generate chimeras. Males with high degree of chimerism were mated to NMRI females for germline transmission. F1 heterozygous males were crossed to NMRI females, and heterozygous offspring were intercrossed.

Mice were genotyped by Southern blotting using a *BamHI* RFLP with the floxed neo-cassette (wildtype allele: 40 kb, mutant: 20 kb), or by PCR, with primers amplifying a 120bp fragment (wildtype) and a 1600bp fragment (mutant) (Supplementary Table 1).

Rhodopsin null mice were obtained from Janis Lem[15]. The following transgenic mouse lines were used: EIIa-Cre[40], Nestin-Cre (Jax: 003771[41]), Pax6α-Cre[27] and GFP-Centrin2[10]. *Ahi1* alleles were denoted as follows: $Ahi1^{-/-}$, $Ahi1^{+/-}$ (homozygous germline null, germline heterozygote: used for all experiments except where indicated otherwise), *Ahi1 Nestin cKO* ($Ahi1^{flox/-}$*Nestin-Cre*+: used for ERGs), *Ahi1 Pax6α cKO* ($Ahi1^{flox/-}$*Pax6α Cre*+, only more peripheral region analyzed: used for generating double mutants with *Nphp1*). All animals were from mixed backgrounds (C57Bl/6, SvJ129, 129/Ola) and compared to littermate or age-matched sibling controls.

Dark-adapted ERG

Mice were tested using previously described methods[42]. Mice dark-adapted overnight were kept under low red lighting and anesthetized by intraperitoneal (IP) injection (10mg/ml ketamine, 1mg/ml xylazine at 0.1ml/10g body weight), dilated with phenylephrine HCl and tropicamide, and kept on a warm pad. Gold loop electrodes on the cornea were referenced to needle electrodes under the cheek, while electrodes clipped to ears served as grounds. Responses were elicited by high intensity flashes (averaged over n=5) at one second intervals over a time base of 500 ms in a Ganzfeld dome with a photostimulator (Model PS22, Grass instrument company, Quincy, MA).

Antibodies and fluorescence microscopy

Mice were anesthetized by isoflurane inhalation and perfused, or eyes were immersed in 4% paraformaldehyde/PBS. 10-25μm cryosections sections corresponding to a medial position (intersecting optic nerve) were stained for immunofluorescence per standard protocols except where noted. We used the following primary antibodies: rabbit anti-Ahi1[43] (1:250, after antigen retrieval by microwaving slides for 15 minutes in 10mM sodium citrate, pH 6.0), mouse anti-acetylated tubulin (Zymed, 6-11B-1, 1:1000), rabbit anti-RPGR (T. Li, 1:1000 on barely fixed tissues as previously described)[44], chicken anti-RP1[45] (1:2000, E.A. Pierce), mouse anti-opsin (1:250, Chemicon). We used Alexa Fluor dyeconjugated secondary antibodies (1:750, Invitrogen/Molecular Probes) and Hoescht 33342 (1:10,000) nuclear dye. Images were obtained on a Fluoview1000 Spectral Deconvolution Confocal microscope (Olympus), under the same parameters/experiment.

Opsin immunofluorescence measurements were determined from raw images using NIH ImageJ software ("Measure RBG" plugin). ONL values were normalized to values from the apical region encompassing IS and OS. Measurements were made on comparable regions of the retina (minimum two/section, from central and peripheral and averaged together, with exception of Pax6a-cre cKOs, for which all measurements were from peripheral/distal regions).

Histology and electron microscopy

For conventional EM, samples were fixed with 2% paraformaldehyde/2% glutaraldehyde/ 0.1M cacodylate buffer and embedded in propylene oxide:Epon 812 resin. Semithin (0.7μm) sections were stained with toluidine blue (0.25% toluidine blue+0.25% sodium borate in water) for light microscopy. Ultrathin sections (70nm) for electron microscopy were collected on copper grids and stained with saturated uranyl acetate and lead citrate solution prior to imaging on a Phillips electron microscope (model 208).

For immuno-electron microscopy, mice were perfused with 4% paraformaldehyde and samples were immersed overnight in 0.1% glutaraldehyde/4% paraformaldehyde/0.1M cacodylate buffer, and embedded in LR White resin (EMS, USA). 70nm sections were etched with saturated sodium periodate and blocked with 4% bovine serum albumin. Sections were incubated with anti-opsin (1D4) primary antibody and with goat anti-rabbit IgG secondary conjugated to 12nm gold (EMS, USA). Sections were subjected to osmium vapour and stained with uranyl acetate and lead citrate. Negative control sections were processed simultaneously and included sections not incubated with primary antibody. Cilia were randomly selected for imaging on a TEM microscope (Zeiss).

In vivo electroporation and 4-OHT treatment

Retinal *in vivo* electroporation at P0 was performed as previously described[21,22] using 5μg/μl total plasmid DNA with 0.01% Fast Green tracer at 0.5μl/eye at the following mass ratios: pCAG-Cre:GFP/pCALNL-DsRed (1:1), and pCAG-ERT2CreERT2/pCALNL-DsRed/pCX-EGFP (2:1:1), but with a modification: DNA solutions were injected through glass micropipets pulled from capillary tubes (World Precision Instruments, TW150F-3). Plasmids were from C. Cepko through Addgene. For ERT2Cre induction, 4-OHT (Sigma,

H7904) was prepared in corn oil (Sigma, C8267) at 2mg/mL and IP injected (400μl/2 week old mouse).

Cell culture and transfection

HEK293T (human embryonic kidney) cells were seeded on 10cm plates and transfected at 90-95% confluency by Lipofectamine2000 (Invitrogen) using 24μg total DNA/plate. Cells were lysed 24 hours later for analysis.

Western blotting and sucrose fractionation

Western blotting was performed on lysates prepared in modified RIPA buffer using the following antibodies: rabbit anti-Ahi1, mouse anti-GFP (Covance, B34), mouse anti-α-tubulin (Sigma, T-6074), and mouse anti-rhodopsin (Chemicon, MAB5316). All antibodies were diluted 1:1000 in 4% milk. Secondary detection was performed using HRP-conjugated anti-mouse or anti-rabbit antibodies (1:20,000, Zymax) in 4% milk. For sucrose fractionation, modified RIPA lysates were loaded onto step-wise gradients from 5% to 60% sucrose followed by ultra-centrifugation overnight at 100,000 *g* force. Fractions were collected from the top and protein was precipitated using trichloro-acetic acid followed by SDS-PAGE and western blotting.

Statistics

For the association studies, two-tailed *P* values were computed using Fisher's exact test by http://www.langsrud.com/fisher.htm using the sum of small *P* values method. The TDT (chi-squared) statistic[34] was computed manually with *P* value assigned for 1 degree of freedom. Relative risk and confidence intervals were computed by http://statpages.org/ctab2x2.html based on a general method[46]. For other studies, data were expressed as means +/− S.E.M. Two-tailed *P* values were calculated by Student's t-test. Values less than 0.05 were considered statistically significant for all tests.

Supplementary Material

Refer to Web version on PubMed Central for supplementary material.

Acknowledgements

We thank Kaylin Siever and Karen Teofilo for assistance with histology; Gabriel Silva, Lingyun Cheng, and Marie Davidson for assistance with ERG testing; Avila Almudena for assistance with clinical data and selecting controls; Janis Lem, Greg Lemke, Tal Burstyn-Cohen, and Anthony Wynshaw-Boris for sharing mice and for feedback and suggestions; Kang Zhang, Lawrence Goldstein, Binhai Zheng for feedback and suggestions; Tiansen Li and Eric Pierce for sharing antibodies; Ching-Hwa Sung for sharing rhodopsin plasmid; Joon Kim and Vincent Cantagrel for technical advice; and Jennifer Meerloo with the UCSD Neurosciences Microscopy Shared Facility (NINDS P30NS047101) for microscopy services and support. This work was supported by the National Institutes of Health R01NS048453 (J.G.G.), P30NS047101 (J.G.G.), F31NS059281 (C.M.L.), R01EY007042 (D.S.W.), UCSD Genetics Training Program institutional training grant, T32 GM008666 from the National Institute for General Medical Sciences (C.M.L. and M.A.L), and the Burroughs Wellcome Fund (J.G.G.). D.S.W. is a Jules and Doris Stein RPB Professor. JGG is an investigator of the Howard Hughes Medical Institute.

References

1. Valente EM, et al. AHI1 gene mutations cause specific forms of Joubert syndrome-related disorders. Ann Neurol. 2006; 59:527–34. [PubMed: 16453322]

2. Parisi MA, et al. AHI1 mutations cause both retinal dystrophy and renal cystic disease in Joubert syndrome. J Med Genet. 2006; 43:334–9. [PubMed: 16155189]
3. Quinlan RJ, Tobin JL, Beales PL. Modeling ciliopathies: Primary cilia in development and disease. Curr Top Dev Biol. 2008; 84:249–310. [PubMed: 19186246]
4. Dixon-Salazar T, et al. Mutations in the AHI1 gene, encoding jouberin, cause Joubert syndrome with cortical polymicrogyria. Am J Hum Genet. 2004; 75:979–987. [PubMed: 15467982]
5. Ferland RJ, et al. Abnormal cerebellar development and axonal decussation due to mutations in AHI1 in Joubert syndrome. Nat Genet. 2004; 36:1008–1013. [PubMed: 15322546]
6. Jiang X, Hanna Z, Kaouass M, Girard L, Jolicoeur P. Ahi-1, a novel gene encoding a modular protein with WD40-repeat and SH3 domains, is targeted by the Ahi-1 and Mis-2 provirus integrations. J Virol. 2002; 76:9046–9059. [PubMed: 12186888]
7. Eley L, et al. Jouberin localizes to collecting ducts and interacts with nephrocystin-1. Kidney Int. 2008; 74:1139–49. [PubMed: 18633336]
8. Hildebrandt F, et al. A novel gene encoding an SH3 domain protein is mutated in nephronophthisis type 1. Nat Genet. 1997; 17:149–153. [PubMed: 9326933]
9. Konrad M, et al. Large homozygous deletions of the 2q13 region are a major cause of juvenile nephronophthisis. Hum Mol Genet. 1996; 5:367–71. [PubMed: 8852662]
10. Higginbotham H, Bielas S, Tanaka T, Gleeson JG. Transgenic mouse line with green-fluorescent protein-labeled Centrin 2 allows visualization of the centrosome in living cells. Transgenic Res. 2004; 13:155–64. [PubMed: 15198203]
11. Wolfrum U, Salisbury JL. Expression of centrin isoforms in the mammalian retina. Exp Cell Res. 1998; 242:10–7. [PubMed: 9665797]
12. Pazour GJ, et al. The intraflagellar transport protein, IFT88, is essential for vertebrate photoreceptor assembly and maintenance. J Cell Biol. 2002; 157:103–13. [PubMed: 11916979]
13. Fliegauf M, et al. Nephrocystin specifically localizes to the transition zone of renal and respiratory cilia and photoreceptor connecting cilia. J Am Soc Nephrol. 2006; 17:2424–33. [PubMed: 16885411]
14. Humphries MM, et al. Retinopathy induced in mice by targeted disruption of the rhodopsin gene. Nat Genet. 1997; 15:216–9. [PubMed: 9020854]
15. Lem J, et al. Morphological, physiological, and biochemical changes in rhodopsin knockout mice. Proc Natl Acad Sci U S A. 1999; 96:736–41. [PubMed: 9892703]
16. Gross AK, et al. Defective development of photoreceptor membranes in a mouse model of recessive retinal degeneration. Vision Res. 2006; 46:4510–8. [PubMed: 16979686]
17. Burns ME, Arshavsky VY. Beyond counting photons: trials and trends in vertebrate visual transduction. Neuron. 2005; 48:387–401. [PubMed: 16269358]
18. Marszalek JR, et al. Genetic evidence for selective transport of opsin and arrestin by kinesin-II in mammalian photoreceptors. Cell. 2000; 102:175–87. [PubMed: 10943838]
19. Deretic D. A role for rhodopsin in a signal transduction cascade that regulates membrane trafficking and photoreceptor polarity. Vision Res. 2006; 46:4427–33. [PubMed: 17010408]
20. Bhowmick R, et al. Photoreceptor IFT Complexes Containing Chaperones, Guanylyl Cyclase 1 and Rhodopsin. Traffic. 2009
21. Matsuda T, Cepko CL. Electroporation and RNA interference in the rodent retina in vivo and in vitro. Proc Natl Acad Sci U S A. 2004; 101:16–22. [PubMed: 14603031]
22. Matsuda T, Cepko CL. Controlled expression of transgenes introduced by in vivo electroporation. Proc Natl Acad Sci U S A. 2007; 104:1027–32. [PubMed: 17209010]
23. Davenport JR, et al. Disruption of intraflagellar transport in adult mice leads to obesity and slow-onset cystic kidney disease. Curr Biol. 2007; 17:1586–94. [PubMed: 17825558]
24. den Hollander AI, Roepman R, Koenekoop RK, Cremers FP. Leber congenital amaurosis: genes, proteins and disease mechanisms. Prog Retin Eye Res. 2008; 27:391–419. [PubMed: 18632300]
25. Liang Y, et al. Rhodopsin signaling and organization in heterozygote rhodopsin knockout mice. J Biol Chem. 2004; 279:48189–96. [PubMed: 15337746]
26. Jiang ST, et al. Essential role of nephrocystin in photoreceptor intraflagellar transport in mouse. Hum Mol Genet. 2009; 18:1566–77. [PubMed: 19208653]

27. Marquardt T, et al. Pax6 is required for the multipotent state of retinal progenitor cells. Cell. 2001; 105:43–55. [PubMed: 11301001]
28. Sunyaev S, et al. Prediction of deleterious human alleles. Hum Mol Genet. 2001; 10:591–7. [PubMed: 11230178]
29. Yue P, Melamud E, Moult J. SNPs3D: candidate gene and SNP selection for association studies. BMC Bioinformatics. 2006; 7:166. [PubMed: 16551372]
30. Sung CH, Schneider BG, Agarwal N, Papermaster DS, Nathans J. Functional heterogeneity of mutant rhodopsins responsible for autosomal dominant retinitis pigmentosa. Proc Natl Acad Sci U S A. 1991; 88:8840–4. [PubMed: 1924344]
31. Tory K, et al. High NPHP1 and NPHP6 mutation rate in patients with Joubert syndrome and nephronophthisis: potential epistatic effect of NPHP6 and AHI1 mutations in patients with NPHP1 mutations. J Am Soc Nephrol. 2007; 18:1566–75. [PubMed: 17409309]
32. Kroes HY, et al. DNA analysis of AHI1, NPHP1 and CYCLIN D1 in Joubert syndrome patients from the Netherlands. Eur J Med Genet. 2008; 51:24–34. [PubMed: 18054307]
33. Caridi G, et al. Renal-retinal syndromes: association of retinal anomalies and recessive nephronophthisis in patients with homozygous deletion of the NPH1 locus. Am J Kidney Dis. 1998; 32:1059–62. [PubMed: 9856524]
34. Spielman RS, McGinnis RE, Ewens WJ. Transmission test for linkage disequilibrium: the insulin gene region and insulin-dependent diabetes mellitus (IDDM). Am J Hum Genet. 1993; 52:506–16. [PubMed: 8447318]
35. Hsiao YC, et al. Ahi1, whose human ortholog is mutated in Joubert syndrome, is required for Rab8a localization, ciliogenesis and vesicle trafficking. Hum Mol Genet. 2009; 18:3926–41. [PubMed: 19625297]
36. Khanna H, et al. A common allele in RPGRIP1L is a modifier of retinal degeneration in ciliopathies. Nat Genet. 2009
37. Caridi G, et al. Nephronophthisis type 1 deletion syndrome with neurological symptoms: prevalence and significance of the association. Kidney Int. 2006; 70:1342–7. [PubMed: 16900087]
38. Koizumi H, Tanaka T, Gleeson JG. Doublecortin-like kinase functions with doublecortin to mediate fiber tract decussation and neuronal migration. Neuron. 2006; 49:55–66. [PubMed: 16387639]
39. Hooper M, Hardy K, Handyside A, Hunter S, Monk M. HPRT-deficient (Lesch-Nyhan) mouse embryos derived from germline colonization by cultured cells. Nature. 1987; 326:292–5. [PubMed: 3821905]
40. Lakso M, et al. Efficient in vivo manipulation of mouse genomic sequences at the zygote stage. Proc Natl Acad Sci U S A. 1996; 93:5860–5. [PubMed: 8650183]
41. Tronche F, et al. Disruption of the glucocorticoid receptor gene in the nervous system results in reduced anxiety. Nat Genet. 1999; 23:99–103. [PubMed: 10471508]
42. El Bradey M, et al. Preventive versus treatment effect of AG3340, a potent matrix metalloproteinase inhibitor in a rat model of choroidal neovascularization. J Ocul Pharmacol Ther. 2004; 20:217–36. [PubMed: 15279727]
43. Lancaster MA, et al. Impaired Wnt-beta-catenin signaling disrupts adult renal homeostasis and leads to cystic kidney ciliopathy. Nat Med. 2009
44. Hong DH, et al. RPGR isoforms in photoreceptor connecting cilia and the transitional zone of motile cilia. Invest Ophthalmol Vis Sci. 2003; 44:2413–21. [PubMed: 12766038]
45. Liu Q, et al. Identification and subcellular localization of the RP1 protein in human and mouse photoreceptors. Invest Ophthalmol Vis Sci. 2002; 43:22–32. [PubMed: 11773008]
46. Fleiss, JL.; Levin, BA.; Paik, MC. Statistical methods for rates and proportions. J. Wiley; Hoboken, N.J.: 2003. p. xxviip. 760

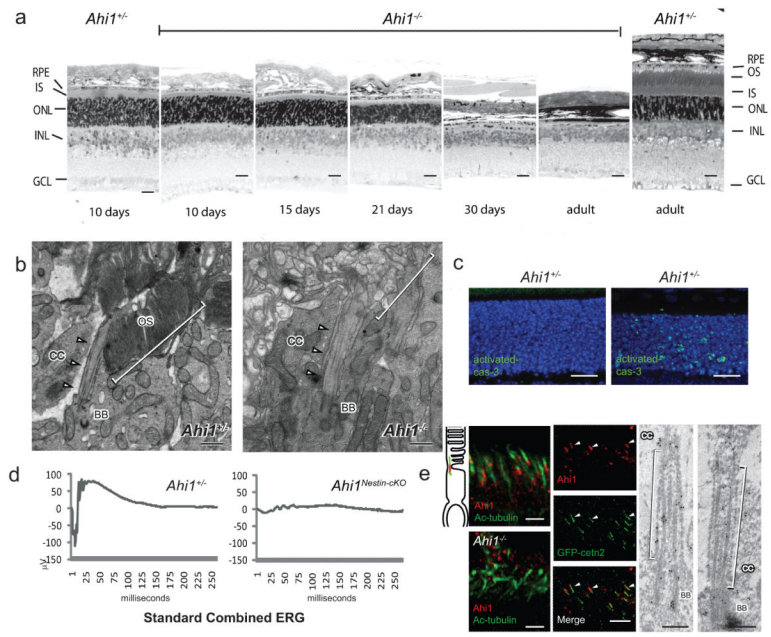

Figure 1.

Degeneration of photoreceptor cells following failed outer segment development in *Ahi1*$^{-/-}$ mouse retina. **(a)** Semi-thin sections of retina stained with toluidine blue from P10 to adult (10 wks) showing acute loss of the outer nuclear layer (ONL) between P21 and P30. Scale=20μm **(b)** Transmission electron microscopy from P10. Outer segments (OS, brackets) are present in *Ahi1*$^{+/-}$, but not in *Ahi1*$^{-/-}$. Connecting cilia (CC, arrowheads) present in both. Scale=0.5 μm **(c)** Photoreceptor cell death is evident before three weeks of age, indicated by activated caspase-3 immunofluorescence (green) from 20μm cryosections. Nuclei are stained with Hoescht 33342 (blue). Shown are representative images from P19 mice, scale=20μm. **(d)** Full field dark-adapted electroretinograms (ERGs) from P19 *Ahi1*$^{flox/-}$*; Nes-Cre+* (*Ahi1*$^{\text{Nestin cKO}}$) and *Ahi1* heterozygous control mice. Shown are representative waveforms from *n*=3-4 mice/genotype. **(e)** Endogenous Ahi1 localization (red) to base of photoreceptor connecting cilium (acetylated-tubulin: green) in *Ahi1*$^{+/-}$ section is absent in *Ahi1*$^{-/-}$ cilium. Ahi1 distribution overlaps with centrin-2 (green) in GFP-Cetn-2 transgenic mouse retina. Arrowheads indicating example GFP-centrin2 labeled connecting cilia, 10μm cryosections, scale=5μm. Ahi1 immunoelectron microscopy from P10 retina, showing particles at the basal body (BB) and along the cilium (CC), scale=0.25μm

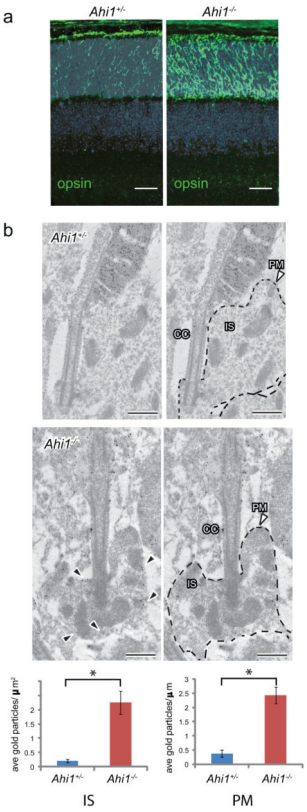

Figure 2.

Opsin accumulation in *Ahi1*−/− photoreceptors **(a)** Opsin immunofluorescence (green) at P10 in $Ahi1^{+/-}$ and $Ahi1^{-/-}$ retina from cryosections. Nuclei are stained with Hoescht 33342. Scale=20μm **(b)** Opsin immunoEM and quantification of immunogold labeling from ultrathin sections of P10 $Ahi1^{+/-}$ and $Ahi1^{-/-}$ retina, *n*=20-23 photoreceptor connecting cilia/genotype. Data are expressed as number of gold particles per μm^2 area within the inner segment (IS, defined as within inner segment and at least 30nm away from PM, *P*=8.0E-06), and as number of particles per μm length of inner segment membranes (PM, dashed lines, *P*=2.2E-07). Black arrowheads indicate examples of abnormally localized opsin, CC=connecting cilium, scale=0.5μm, error bars represent s.e.m.

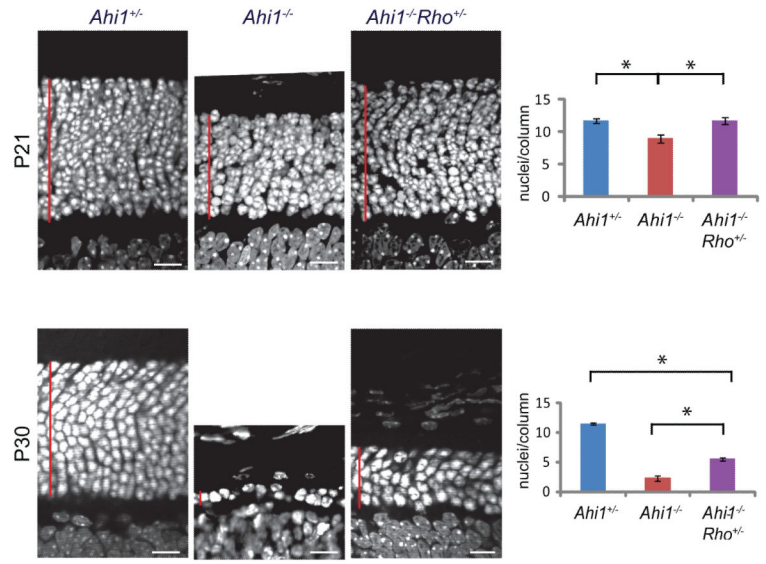

Figure 3.

Opsin contributes to cell death in *Ahi1*$^{-/-}$ mice. 10μm cryosections from P21 and P30 retina showing delay of cell loss associated with reduced opsin dosage (*Ahi1*$^{-/-}$*Rho*$^{+/-}$), measured as average number of cells/column (nuclei were stained with Hoescht 33342 and counts expressed as average of three counts across each section). Asterisk in top panel denotes significant difference from both control and rescue, *n*=3-7, *P*=0.00175 (P21) and 0.00613 (P30), scale=10μm, error bars represent s.e.m.

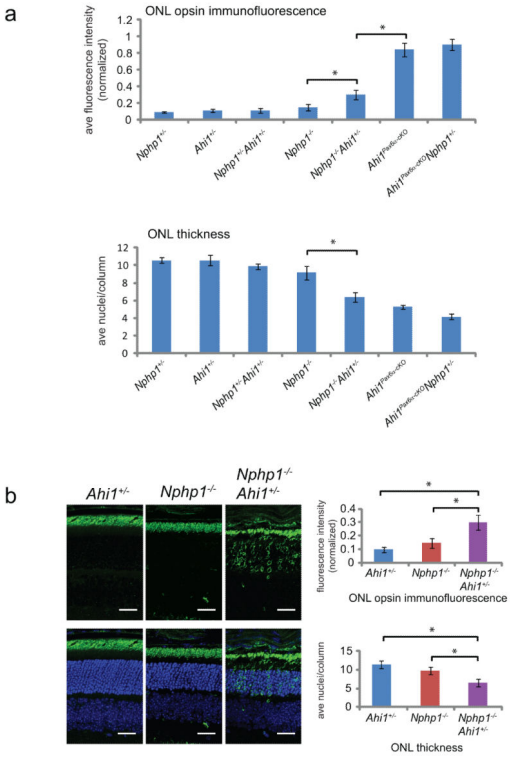

Figure 4.

Genetic interaction of *Ahi1* with *Nphp1*. **(a)** Increased cell loss and redistribution of opsin with increased load of deleterious *Ahi1* and *Nphp1* mutations in mouse retina. Quantification of opsin immunofluorescence(green) from ONL (outer nuclear layer, normalized as ratio of ONL:apical region encompassing IS and OS), and quantification of outer nuclear layer (ONL) thickness, expressed as averaged number of nuclei/column (indicated by Hoescht 33342 staining) from 10μm cryosections from indicated genotypes at P21. **(b)** From part (a), *Ahi1* null allele modifies the $Nphp1^{-/-}$ phenotype, with $Nphp1^{-/-}Ahi1^{+/-}$ showing increased opsin accumulation and decreased thickness of the ONL versus $Nphp1^{-/-}$ and $Ahi1^{+/-}$ controls. Asterisk denotes significant difference from both $Ahi1^{+/-}$ and $Nphp1^{-/-}$, n=6-7, P(ONL thickness)=0.00315 and 0.000106, respectively; and P(fluorescence)=0.0454 and 0.0141, respectively, scale=20μm, error bars represent s.e.m.

Table 1

Frequency of AHI1 p.R830W (c.C2488T) in Italian cases affected with nephronophthisis with or without additional retinal involvement

	2N	N	genotypes			genotype frequency			alleles		allele frequency		P	
Groups			**CC**	**CT**	**TT**	**f(CC)**	**f(CT)**	**f(TT)**	**C**	**T**	**f(C)**	**f(T)**	**vs. total controls***	**RD vs. non-RD**
Total Controls	612	306	289	17	0	0.944	0.056	0	595	17	0.927	0.028		
NPHP	274	137	132	5	0	0.964	0.036	0	269	5	0.982	**0.018**	ns	
NPHP+RD	32	16	8	8	0	0.500	0.500	0	24	8	0.750	**0.250**	**9.03E-06**	**5.36E-06**
Total NPHP	306	153	140	13	0	0.915	0.085	0	293	13	0.958	0.042	ns	
NPHP1	74	37	37	0	0	1.000	0.000	0	74	0	1.000	0.000	ns	
NPHP1+RD	10	5	2	3	0	0.400	0.600	0	7	3	0.700	0.300	0.0029	0.0013
Total *NPHP1* ¥	84	42	39	3	0	0.929	0.071	0	81	3	0.964	0.036	ns	
non-NPHP1	200	100	95	5	0	0.950	0.050	0	195	5	0.975	0.025	ns	
non-NPHP1+RD	22	11	6	5	0	0.545	0.455	0	17	5	0.773	0.227	0.00056	0.0011
Total non-*NPHP1* ¥	222	111	101	10	0	0.910	0.090	0	212	10	0.955	0.045	ns	

* two tailed *P* values greater than 0.05 were considered not significant, **ns** RD= retinal degeneration

¥ *NPHP1* refers to NPHP patients with mutations in the *NPHP1* gene, non-*NPHP1* refers to NPHP patients excluded for mutations in *NPHP1*

Nat Genet. Author manuscript; available in PMC 2010 August 01.